JACS
JOURNAL OF THE AMERICAN CHEMICAL SOCIETY
pubs.acs.org/JACS
Article

Dissociative Transition State in Hepatitis Delta Virus Ribozyme Catalysis

Benjamin Weissman, Şölen Ekesan, Hsuan-Chun Lin, Shahbaz Gardezi, Nan-Sheng Li, Timothy J. Giese, Erika McCarthy, Michael E. Harris,* Darrin M. York,* and Joseph A. Piccirilli*

Cite This: J. Am. Chem. Soc. 2023, 145, 2830–2839
Read Online
ACCESS | Metrics & More | Article Recommendations | Supporting Information

ABSTRACT: Ribonucleases and small nucleolytic ribozymes are both able to catalyze RNA strand cleavage through 2′-*O*-transphosphorylation, provoking the question of whether protein and RNA enzymes facilitate mechanisms that pass through the same or distinct transition states. Here, we report the primary and secondary ^{18}O kinetic isotope effects for hepatitis delta virus ribozyme catalysis that reveal a dissociative, metaphosphate-like transition state in stark contrast to the late, associative transition states observed for reactions catalyzed by specific base, Zn^{2+} ions, or ribonuclease A. This new information provides evidence for a discrete ribozyme active site design that modulates the RNA cleavage pathway to pass through an altered transition state.

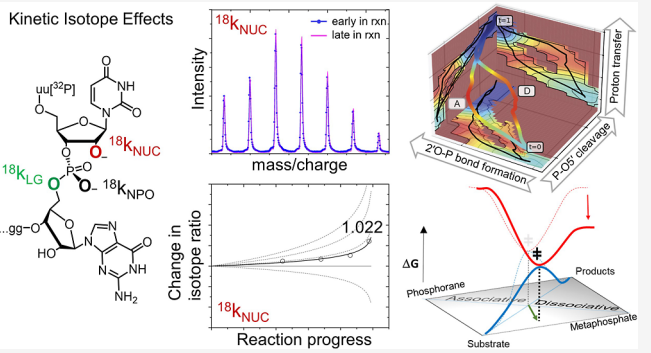

Downloaded via RUTGERS UNIV on February 8, 2023 at 20:55:15 (UTC).
See https://pubs.acs.org/sharingguidelines for options on how to legitimately share published articles.

INTRODUCTION

Enzymes stabilize reaction transition states;[1] therefore, a predictive understanding of the transition state structure and bonding is essential to gain insight into the catalysis and to guide the design of inhibitors or new enzymes for biotechnology, diagnostics, or therapeutics.[2,3] Both RNA and protein enzymes can stabilize the transition states for phosphoryl transfer reactions and are proposed to use similar catalytic strategies.[4,5] However, there are relatively little experimental data that directly report on the transition states of RNA transphosphorylation reactions catalyzed by either ribonucleases or ribozymes. Only comparative analysis at the level of transition state structure can resolve a fundamental question: are the pathways for RNA transphosphorylation restricted by the free energy landscape of the reaction such that biology converged on a single catalytic solution, or do multiple biologically feasible routes to cleavage exist that pass through fundamentally different transition states?

Highly sensitive experimental probes of transition state structure and bonding are kinetic isotope effects (KIEs) on the reaction rate.[6−8] Herein, we report the primary and secondary ^{18}O KIEs for RNA cleavage catalyzed by the hepatitis delta virus ribozyme (HDVr). RNA cleavage by 2′-*O*-transphosphorylation is ubiquitous in biology, shapes the terrestrial transcriptome,[4,9,10] and has far-reaching implications for medicine.[11,12] A predictive understanding of the catalytic mechanisms of RNA cleavage reactions is thus important from a fundamental scientific perspective as well as from the standpoint of engineering novel catalysts.[13,14] HDVr is a representative class of nucleolytic ribozymes[15,16] that serve as platforms for the design of new biomedical technology[14] and therapeutics[11,12] and as models for understanding RNA catalysis[17] and its implications for theories of evolution.[18] The KIE measurements reported here are the first for any nucleolytic ribozyme and afford a unique opportunity to determine whether the catalytic pathways of RNA enzymes pass through transition states like those of protein ribonucleases. In this way, insight can be gained into the degree to which the transition state structure can vary in these distinct catalytic environments.

The 2′-*O*-transphosphorylation reaction comprises two main bonding events: association of the 2′O nucleophile (A_N) and dissociation of the 5′O leaving group (D_N). The order and extent of these two events leading to the transition state can vary and are illustrated within these two dimensions in Figure 1a.[19] Mechanisms are referred to as associative (or dissociative) when the primary association (or dissociation) event proceeds first and as concerted when they occur simultaneously. Purely associative/dissociative mechanisms are stepwise with a metastable intermediate separating two transition states, whereas a purely concerted mechanism will pass through a single transition state. Transition states along a given mechanistic path are described as “early” or “late” based

Received: September 21, 2022
Published: January 27, 2023

© 2023 American Chemical Society

https://doi.org/10.1021/jacs.2c10079
J. Am. Chem. Soc. 2023, 145, 2830−2839

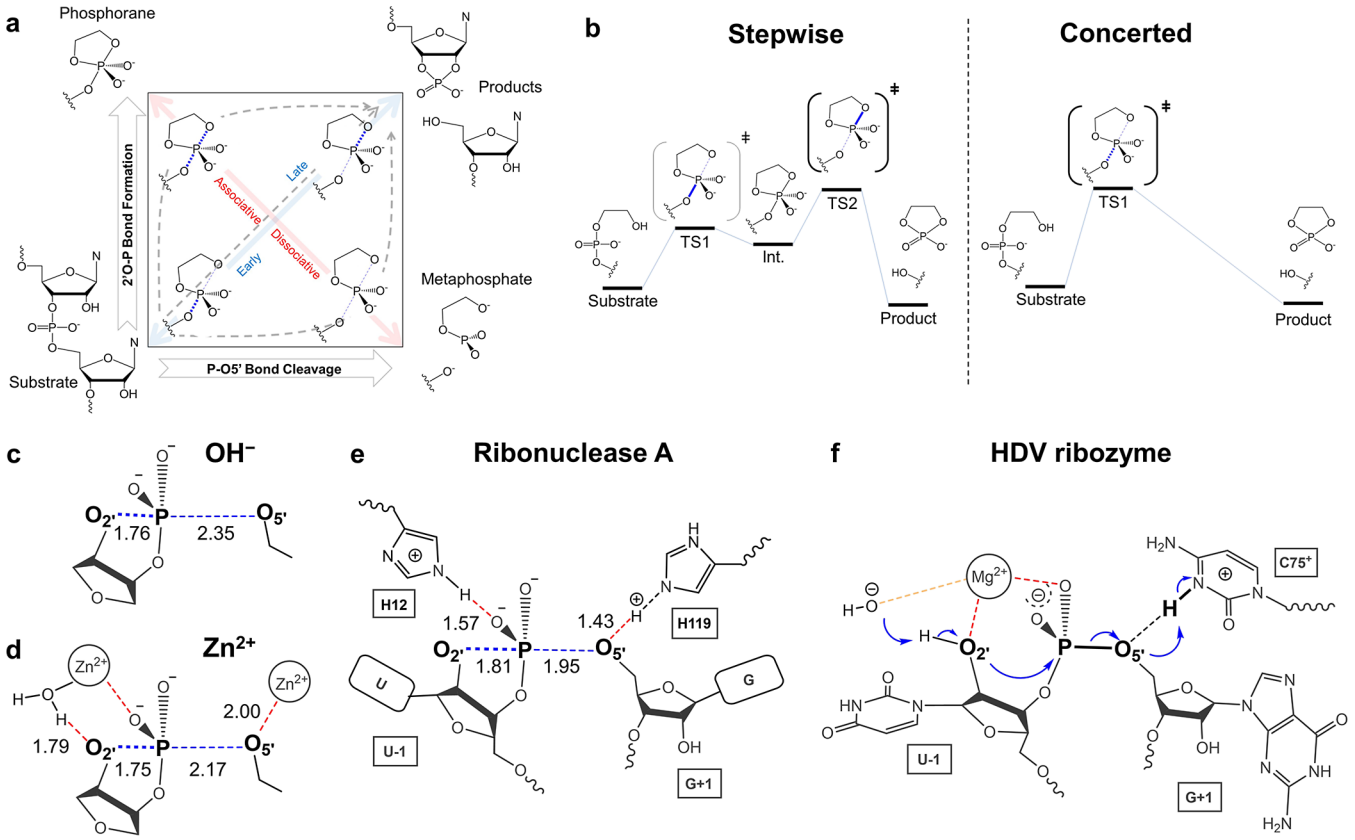

Figure 1. Transition states for RNA cleavage and where to find them. (a) Two-dimensional reaction coordinate diagram with 5′O−P bond breaking and 2′O−P bond formation proceeding along the horizontal and vertical axes, respectively. Regions of transition states for associative versus dissociative (red diagonal) pathways having early versus late (blue diagonal) character are shown inside the box, whereas metastable intermediates are depicted outside the box. Potential concerted reaction pathways are shown as gray dashed lines. Stepwise mechanisms with either phosphorane or metaphosphate intermediates proceed sequentially along individual axes. (b) Two classes of the transphosphorylation mechanism: stepwise with an intermediate (Int.) and two transitions states (TS1 and TS2) and concerted with a single TS1. (c−e) Experimentally guided, computationally derived transition state models of RNA 2′-*O*-transphosphorylation consistent with ^{18}O KIEs reported previously (Table 1) for reactions catalyzed by (c) specific base (OH^-), (d) Zn^{2+} ions, and (e) RNase A. Key distances in Å are indicated. (f) Catalytic mechanism of HDVr showing the proposed roles of protonated C75 acting as a general acid and active site Mg^{2+} ion coordinated to a non-bridging phosphoryl oxygen and participating in catalysis via coordination of the 2′O (red) or as general base via a coordinated hydroxide (orange).

on whether they are closer to the reactant or product states, respectively. However, distinctions between pure mechanisms are not always clear; for example, when a metastable intermediate on the free energy surface is not kinetically distinguishable from a "shoulder" formed from the coalescence of two transition states into one. Based on Brønsted analyses, KIEs, and quantum mechanical (QM) calculations,[20] the mechanisms of transphosphorylation reactions can be concerted with early transition states for substrates with reactive (enhanced) leaving groups like *p*-nitrophenol with low pK_a; however, the high pK_a of RNA's 5′O leaving group typically results in mechanisms with more associative character, in which leaving group departure through cleavage of the 5′O−P bond is rate-limiting and the corresponding transition state is late (Figure 1b).

As will be revealed in this study, the HDVr-catalyzed RNA cleavage reaction proceeds through a dissociative-like pathway and transition state characterized by minimal bond formation between the O2′ nucleophile and the scissile phosphate. This is in stark contrast to the late, associative-like transition states characterized by nearly complete O2′−P bond formation experimentally observed for reactions catalyzed by a specific base,[21,22] Zn^{2+} ions,[23,24] and ribonuclease A[21,25] (RNase A) (Figure 1c−f) and computationally predicted for classes of small self-cleaving ribozymes[26] that employ a guanine general base.[16,27]

RESULTS AND DISCUSSION

RNA 2′-*O*-Transphosphorylations Catalyzed by OH^-, Zn^{2+} Ions, and RNase A Proceed by Associative Mechanisms. A powerful method to gain insight into the mechanism and transition state structure is to determine KIEs on reacting substrate atoms and use the results as benchmarks for evaluating alternative mechanisms and transition states.[6] The rate effect of isotopic substitution reports directly on changes to the bonding environment around the substituted atom between the ground state and transition state (for ^{18}O substitutions, mainly due to differences in vibration zero-point energies).[7] KIEs in model systems, together with QM calculations, provide guidance on how to interpret enzyme KIEs.[19,22] KIE analysis has been applied to RNA catalysts that catalyze chemistry at carbon centers, including the ribosome[28] and the pyrimidine-forming ribozyme[29] but not yet to endonucleolytic ribozymes that catalyze RNA-2′-*O*-transphosphorylation. Importantly, KIEs were previously measured and interpreted by computational simulations for the reactions

https://doi.org/10.1021/jacs.2c10079
J. Am. Chem. Soc. 2023, 145, 2830−2839

Table 1. Available Experimental and Calculated KIE Values for RNA Backbone Cleavage by 2′-*O*-Transphosphorylation Reactions[a]

substrate	catalyst	pH	$^{18}k_{NUC}$	*n*	$^{18}k_{LG}$	*n*	$^{18}k_{NPO}$	*n*	refs
UpG	H_3O^+	1[b]	0.990 (4)		1.005 (4)		0.991 (1)		21
UpG	OH^-	12[b]	0.996 (2)		1.037 (2)		0.999 (1)		21
UpG	OH^-	12[b]	0.997 (1)		1.034 (3)		0.999 (1)		24
UpG	OH^-	14[b]	0.984 (3)		1.034 (4)				21
UpG	Zn^{2+}	7[c]	0.986 (3)		1.015 (1)		1.007 (2)		24
UpG	RNase A	7	0.994 (2)		1.014 (3)		1.001 (1)		21
HPPNP	OH^-	12	1.0327 (8)		1.0064 (9)				49
UpG	OH^- (Calc. Assoc.)		0.977		1.042		1.004		26
UpG	Zn^{2+} (Calc. Assoc.)		1.001		1.032		1.002		23
UpG	RNase A (Calc. Assoc.)		0.993		1.028		1.002		26
11 mer	HDVr (RL)		1.024 (1)	93	1.017 (3)	26	0.994 (4)	27	CW
11 mer	HDVr (MS)		1.026 (6)	4					CW
9 mer	HDVr (Calc. Dissoc.)		1.025		1.018		1.003		CW
9 mer	HDVr (Calc. Assoc.)		0.999		1.006		1.002		CW

[a]"*n*" is the number of experimental replicates. "RL" and "MS" correspond to KIE obtained by remote label and mass spectrometry methods, respectively. The standard error in the last significant figure for the experimental KIEs is given in parenthesis. Calculated ^{18}O KIE values (Calc.) for associative-like and dissociative-like HDVr mechanisms were obtained from the Bigeleisen−Mayer equation[50] using vibrational frequencies obtained with PBE0/6-31G* QM/MM Hessians. "CW" indicates new measurements presented in the current work. [b]KIEs were measured at 1 M Na^+ adjusted with NaCl at 37 °C. [c]The KIEs for Zn^{2+} and (OH^-) catalysis compared at 0.1 M $NaNO_3$ at 90 °C.

catalyzed by H_3O^+,[21] OH^-,[21,24] Zn^{2+} ions,[23,24] and RNase A[21,25,26] as summarized in Table 1.

In solution, RNA 2′-*O*-transphosphorylation at low pH occurs via an associative stepwise mechanism (A_N + D_N) beginning with protonation of a non-bridging phosphoryl oxygen in the ground state and proceeding through a phosphorane monoanion intermediate, as evidenced by the formation of isomerization products.[30] The rate-limiting breakdown of phosphorane is reflected in inverse KIE values for the nucleophile ($^{18}k_{NUC}$ ∼ 0.990) and non-bridging oxygens (NPOs) ($^{18}k_{NPO}$ ∼ 0.991) and a small normal leaving group KIE ($^{18}k_{LG}$ ∼ 1.005). In contrast, base catalysis proceeds by an (asynchronous) concerted (A_ND_N) mechanism[30] with associative character and a late product-like transition state (Figure 1c). For this mechanism, inverse KIE values for ^{18}O-substitution of the nucleophile ($^{18}k_{NUC}$ ∼ 0.98) and normal leaving group KIEs ($^{18}k_{LG}$ ∼ 1.03) are observed.[20,31] Experimental and computational evidence shows that RNA cleavage catalyzed by RNase A proceeds via a similar mechanism and transition state marked by a slightly less normal leaving group KIE ($^{18}k_{LG}$ ∼ 1.014) that is similar to catalysis by Zn^{2+} ions despite over 10^{10}-fold rate enhancement by the enzyme.[21] In each case, the reaction is initiated with the association of the nucleophile, and the transition states are characterized by advanced O2′−P bond formation, consistent with inverse KIE values ($^{18}k_{NUC}$ < 1) (Table 1). Only in the case of hydroxypropyl *p*-nitrophenol phosphate (HPPNP), in which an enhanced leaving group is introduced, is the transition state early (relatively less O2′−P bond formation) and the $^{18}k_{NUC}$ normal.

Kinetic Isotope Effect Measurements Suggest That HDVr-Catalyzed RNA 2′-*O*-Transphosphorylation Proceeds by a Dissociative-like Mechanism. Due to the lack of data reporting directly on the transition states for RNA enzymes, it remains an open question in the field as to whether nucleolytic ribozymes, having more limited chemical diversity from which to enable different catalytic strategies,[4,5] navigate this mechanistic landscape in similar or distinct ways compared to their protein enzyme counterparts (ribonucleases). A well-studied example, HDVr, also catalyzes 2′-*O*-transphosphorylation (Figures 1f and 2a). A wealth of data including high-resolution crystal structures[32−34] and computational models[35−39] support a mechanism involving C75 (genomic)/C76 (antigenomic) acting as a general acid analogous to His119 of RNase A. Key biochemical support is derived from the rescue of C75/76 mutants by cytosine and imidazole analogues[40] as well as by a 5′-phosphorothiolate modification linking nucleobase protonation to leaving-group stabilization.[41] Thio-effects, metal ion rescue, and Raman crystallography[42−45] experiments suggest inner-sphere contact between the pro-R_P non-bridging phosphoryl oxygen and a metal ion[46,47] that is likely also to play a role in the activation of the nucleophile.[34,35] Brønsted analysis suggests that 2′O develops a negative charge in the transition state, implying that deprotonation precedes 2′O−P bond formation.[48] Although much is known about the functional interactions that facilitate catalysis, there is little experimental information about the HDVr transition state itself, which would serve to validate proposed catalytic pathways.[37,47] To resolve this limitation, we measured the 2′O, 5′O, and non-bridging phosphoryl oxygen KIEs for HDVr and used known mechanistic features together with computational methods to interpret the transition state structure and bonding.

KIEs for HDVr were measured by internal competition[8] in reactions containing mixtures of ^{16}O- or ^{18}O-labeled substrates. We synthesized HDVr 11-mer RNA substrates enriched with ^{18}O at the 2′O, 5′O, and NPO positions to measure $^{18}k_{NUC}$, $^{18}k_{LG}$, and $^{18}k_{NPO}$, respectively (Figure 2b). To detect changes in isotope ratios, we first used a remote label method in which the heavy or light isotope is distinguished by radioactive 5′ end labeling with either ^{32}P or ^{33}P. The products and residual precursor were isolated by PAGE and isotope ratios determined by liquid scintillation counting. To validate the method, we reproduced KIE measurements for base-catalyzed hydrolysis in an 11 mer oligonucleotide substrate containing a single ribose linkage at the isotopically enriched phosphate. The pH dependence and pK_a for cleavage of the 11 mer agree with those measured for the dinucleotide model system

https://doi.org/10.1021/jacs.2c10079
J. Am. Chem. Soc. 2023, 145, 2830−2839

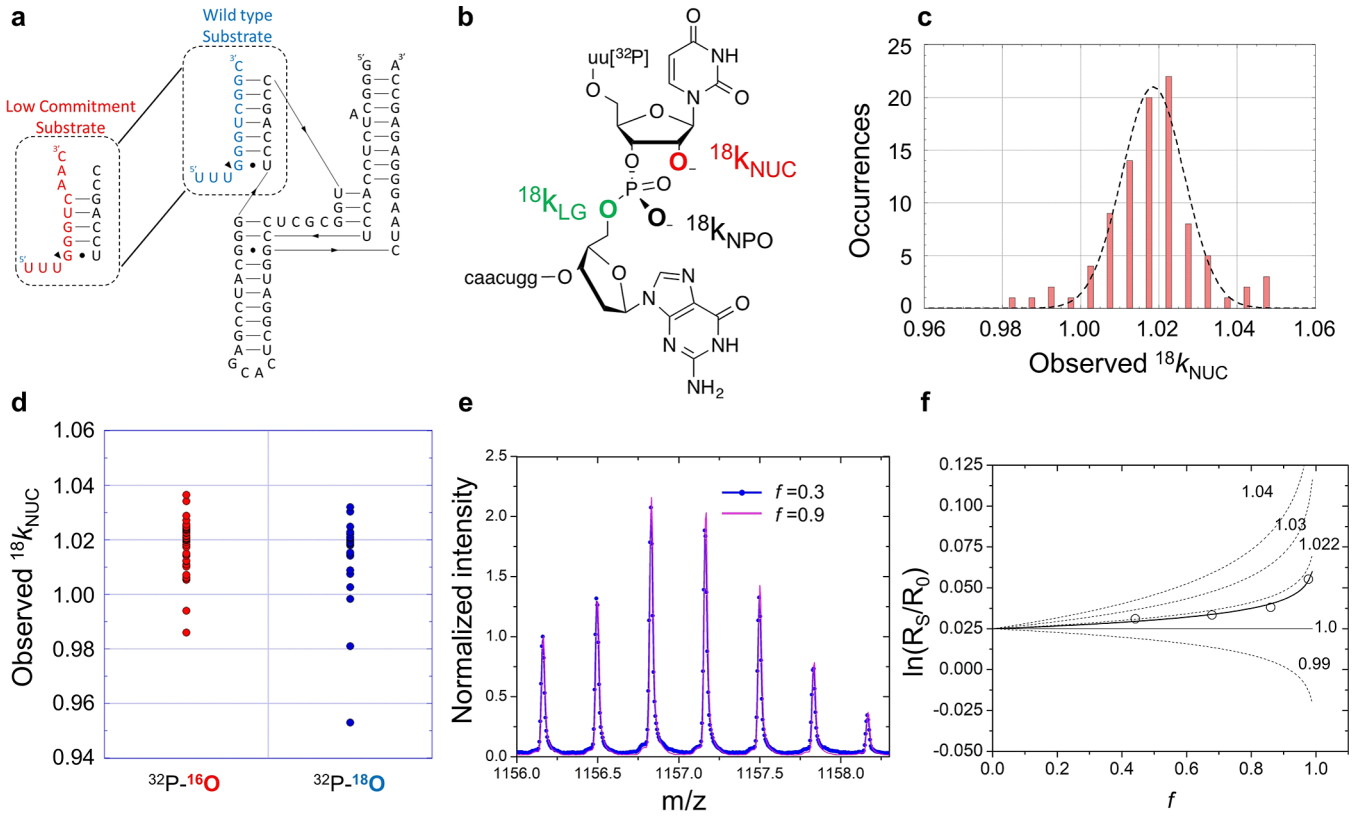

Figure 2. Normal $^{18}k_{NUC}$ for HDVr-catalyzed RNA 2′-*O*-transphosphorylation determined by two alternative methods (a) sequence and secondary structure of HDVr (black), the wildtype substrate (blue), and the mutant substrate with low binding commitment (red, see the Supporting Information). (b) Positions of ^{18}O-substitution for measurements of $^{18}k_{NUC}$ (red), $^{18}k_{LG}$ (green), and $^{18}k_{NPO}$ (black). (c) Distribution of individual measurements of $^{18}k_{NUC}$ by the ^{32}P/^{33}P remote label. The data set is fit to a Gaussian distribution (dotted line) with a peak centered at 1.019 matching the observed KIE (Table S1). The intrinsic $^{18}k_{NUC}$ corrected for commitments and isotopic enrichment of the ^{18}O substrate is reported in Table 1. (d) Comparison of the distribution of $^{18}k_{NUC}$ measurements for opposite remote labeling orientation with ^{32}P labeled 2′-^{16}O substrate (red) versus with ^{32}P labeled on the 2′-^{18}O substrate RNA (blue). (e) ESI-TOF mass spectrum of a mixture of 2′-^{18}O and 2′-^{16}O substrate RNA reacting with HDVr at f = 0.9 (magenta) and f = 0.3 (blue) demonstrating enrichment in 2′-^{18}O in the residual substrate consistent with a normal $^{18}k_{NUC}$. (f) Determination of $^{18}k_{NUC}$ from fitting the change in the isotope ratio of the residual substrate (R_0 = ^{18}O/^{16}O ratio in the 11 mer substrate starting population; R_S = ^{18}O/^{16}O ratio in the residual 11 mer substrate at a fraction of reaction f) as a function of reaction progress, f. Simulated data for KIEs of 0.99, 1.0, 1.022, 1.03, and 1.04 are shown as dotted lines. Fitting of the experimental data to $\ln(R_S/R_0) = (1/^{18}k - 1)\ln(1 - f) + \ln(R_0)$, where ^{18}k is the isotope effect and f is the fraction of the substrate consumed as determined by HPLC (solid line).

(Figure S1). KIEs measured by remote label match previous measurements by mass spectrometry, although a less normal $^{18}k_{LG}$ value was obtained for the 11 mer oligonucleotide compared to the dinucleotide system (Table S1). The $^{18}k_{LG}$ was measured to be 1.037 (2) in 1 M Na^+ at 37 °C and 1.034 (3) in 0.1 M $NaNO_3$ at 90 °C, while the 11 mer effect was 1.019 (3) in 1 M Na^+ at 25 °C. Potentially, the greater local charge density in the oligonucleotide may preferentially accumulate cations able to offset negative charge accumulation to alter the observed KIE. Nonetheless, while the origin of the differences in $^{18}k_{LG}$ remains unclear, the remote label approach returns substantial normal and inverse values for $^{18}k_{LG}$ and $^{18}k_{NUC}$, respectively, for the non-enzymatic base-catalyzed reaction of the 11 mer oligonucleotide, which serve as a reference for the HDVr results. Importantly, pairing of remote labels with substrates did not affect the KIE measurement (^{32}P−^{16}O/^{33}P−^{18}O or reverse) (Figure 2c,d).

For enzyme KIEs measured by competitive methods, substrate binding steps may interfere with measurements.[6] If substrate dissociation is slow relative to the chemistry, resulting in a "commitment" of the bound substrate to undergo chemical transformation, this will attenuate the observed KIEs relative to their intrinsic values. Therefore, conditions where substrate dissociation is fast relative to the chemistry are preferred. To increase the rate constant for substrate dissociation and decrease the forward commitment to catalysis, two base pairs distal to the cleavage site were disrupted (Figure 2). Product formation was quantified using 5′-^{32}P end-labeled 11 mer substrate RNA resolved by PAGE. Single turnover pulse-chase experiments showed that dissociation is rapid with respect to catalysis for the 11 mer substrate (Figure S2). The KIEs for HDVr (Table 1) indicate that the chemical step is at least partially rate-limiting and consistent with minimal binding commitments.

The remote label method permits determination of sufficient trials to fit the data to a normal Gaussian distribution (Figure 2c). Remarkably, we observed a normal KIE of 1.024 (1) for the 2′O nucleophile. Importantly, the same normal $^{18}k_{NUC}$ for HDVr is observed for the opposite remote labeling scheme, demonstrating that the identity of the remote label does not contribute to the observed KIE. A normal nucleophile KIE was surprising since $^{18}k_{NUC}$ for non-enzymatic reactions and RNase A are characteristically inverse (Figure 1e and Table 1), suggestive of advanced 2′O−P bond formation in the

https://doi.org/10.1021/jacs.2c10079
J. Am. Chem. Soc. 2023, 145, 2830−2839

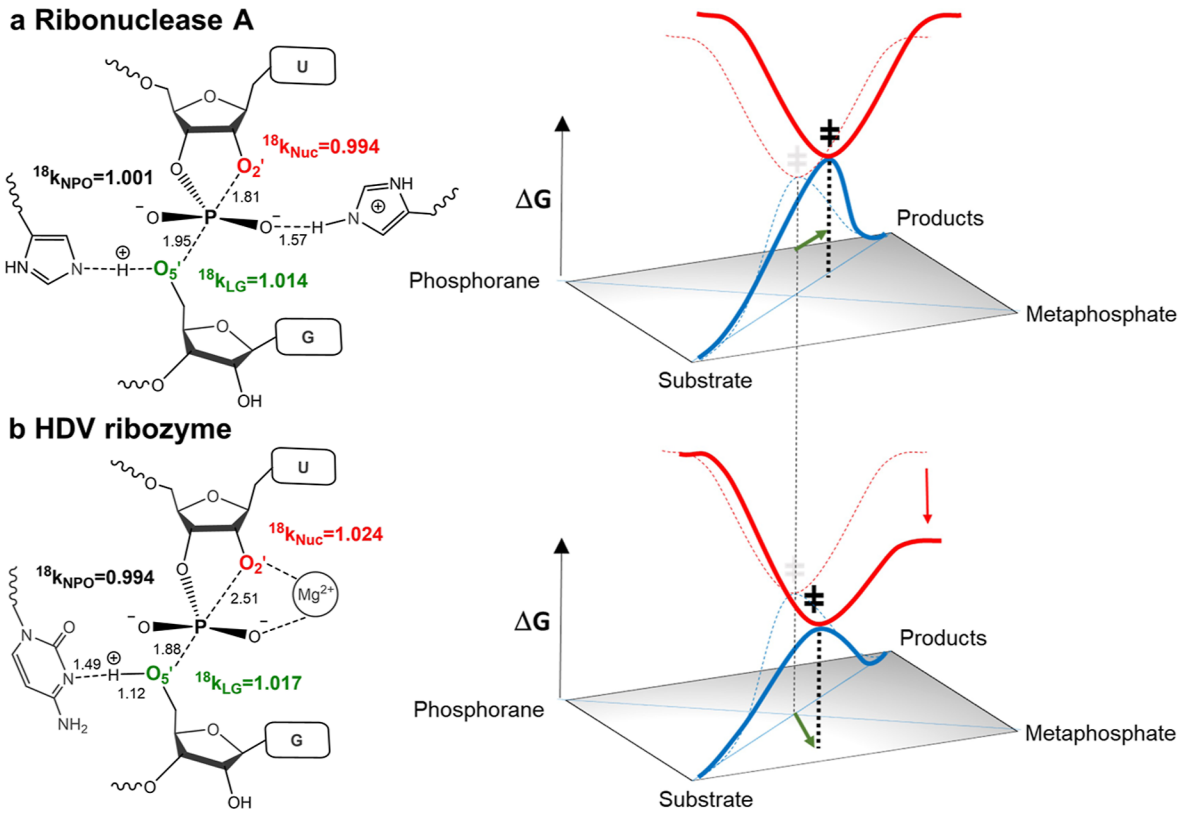

Figure 3. Comparison of idealized free energy surfaces for RNA 2′-*O*-transphosphorylation reactions catalyzed by RNase A (a) and HDVr (b). Experimental KIEs and calculated TS distances are depicted on the left. Transition state locations that correspond to the maxima of the one-dimensional substrate-to-product coordinate (blue) and the minima on the orthogonal coordinate (red), with the corresponding ideal non-enzymatic path (i.e., passing through a symmetric dianionic phosphorane TS) used for reference (transparent dotted lines), are illustrated on the right. (a) RNase A provides extraordinary rate enhancement by using acid/base catalysis to stabilize a transition state that is similar to non-enzymatic reactions under alkaline conditions as inferred by KIEs. (b) HDVr provides rate enhancement using a combination of nucleobase and metal ion catalytic interactions. The free energy surface is distorted relative to ideal non-enzymatic reactions and RNase A toward a dissociative path and metaphosphate-like transition state marked by limited 2′O−P bond formation. These surfaces and pathways are meant to be illustrative, with the relative heights of the enzymatic and ideal non-enzymatic TSs normalized such that their locations on the surface are clearer.

transition state. Additionally, a normal $^{18}k_{NUC}$ for transphosphorylation is only observed for reactions of HPPNP in which the transition state is early due to a more reactive leaving group. Therefore, we determined $^{18}k_{NUC}$ independently using direct analysis of isotope ratios by mass spectrometry. The residual precursor RNAs were analyzed by electrospray ionization time of flight mass spectrometry (ESI-TOF MS), and the isotopic envelope of the entire ion cluster was used to determine the isotope ratios (Figure 2e). The sensitivity and precision of the ESI-TOF MS measurements were established by dilution of natural abundance 11 mer RNA (Figure S3). The KIE is observed as a change in the relative ratios of the product ions containing only natural abundance ^{18}O at all oxygens (M) and those enriched in ^{18}O at one of the reacting phosphoryl oxygens (M + 2). Figure 2f shows the determination of KIEs for HDVr-catalyzed 2′-*O*-transphosphorylation relative to simulations of $^{18}O/^{16}O$ ratio vs f (the fraction of substrate 11 mer reacted to form a product) for a range of potential ^{18}O KIEs. The measurement of $^{18}k_{NUC}$ using direct determination of isotope ratios using mass spectrometry confirms the normal nucleophile KIE for the HDVr.

The $^{18}k_{NUC}$ for HDVr catalysis is 1.024 and contrasts to 0.984 for the non-enzymatic reaction catalyzed by specific base (Table 1). The large inverse value for the non-enzymatic reaction reflects an oxyanion ground state and advanced bond formation in the transition state, consistent with a large β_{NUC} for hydroxide-catalyzed cleavage and computation.[20,51] With respect to metal ion interactions, coordination by divalent metal ions may result in a stiffer binding environment for the interacting oxygen atom,[52] which would also contribute to an inverse KIE. However, secondary ^{18}O isotope effects for hexokinase-catalyzed phosphoryl transfer show that for Mg^{2+} coordination, the effect may be no larger than 1.001.[53] Deprotonation of the 2′O will make a normal contribution to the observed KIE offsetting contributions due to O−P bonding. A value of 1.024 for the equilibrium isotope effect (EIE) on 2′OH deprotonation ($^{18}K_{eq}$) was reported by Humphry et al. from ab initio calculations on the deprotonation of the hydroxyl of 2-hydroxypropyl-*p*-nitrophenyl phosphate.[49] This value matches the estimate for the $^{18}K_{eq}$ for 2′OH of ribose based on the difference in the observed pH dependence of $^{18}k_{NUC}$ for specific base catalysis of RNA-catalyzed 2′-*O*-transphosphorylation above and below its pK_a.[22] A breakpoint in the pH dependence of the reaction rate above pH 13 is observed for RNA cleavage that reflects the pK_a of the 2′O nucleophile. Above the breakpoint (pH 14), the ground state for the reaction is the 2′ oxyanion and the $^{18}k_{NUC}$ is 0.984 (Table 1). A smaller nucleophile KIE is observed at pH 12 (0.997) that is the combined effect of the EIE on 2′OH deprotonation (ca. 1.02) and the intrinsic KIE on the

https://doi.org/10.1021/jacs.2c10079
J. Am. Chem. Soc. 2023, 145, 2830−2839

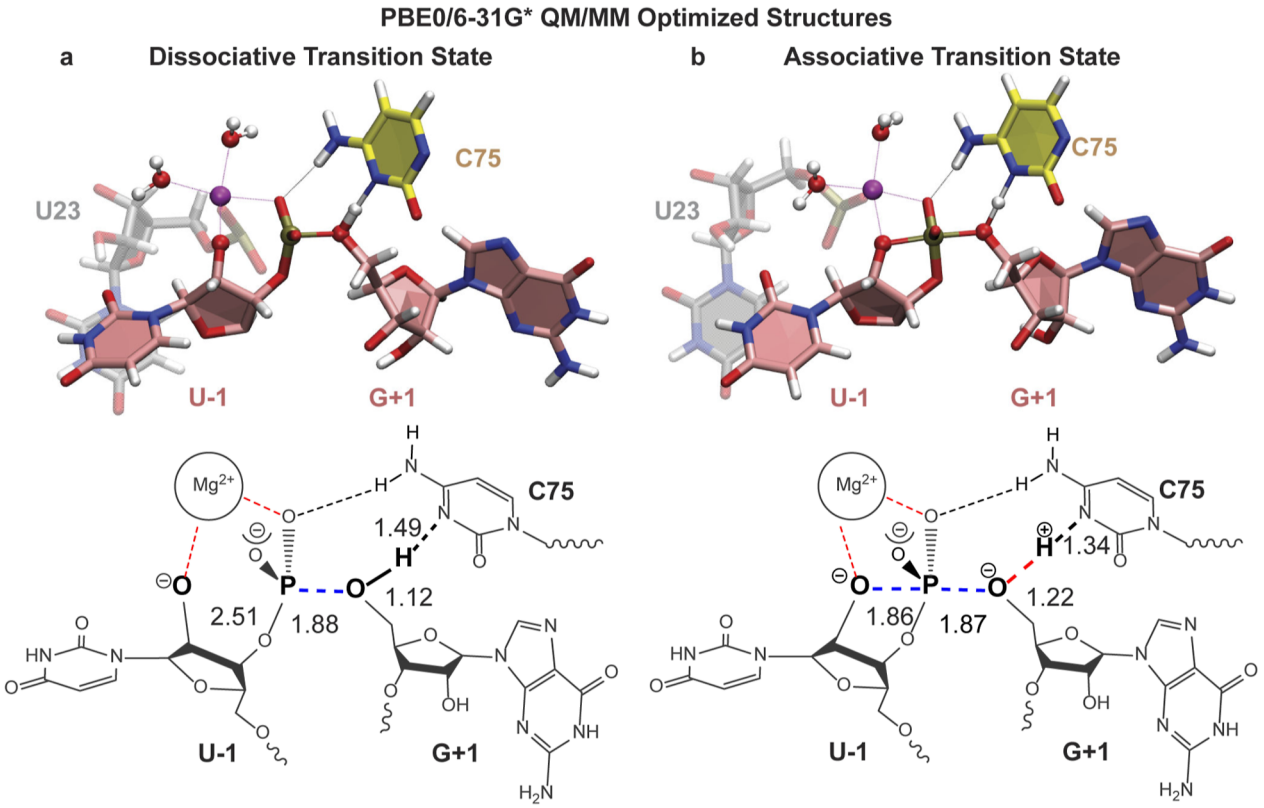

Figure 4. Summary of computational results. Structural description of the transition states obtained by the dissociative (a) and associative (b) reaction pathways found by string simulations and further geometry optimized using PBE0/6-31G* for QM description.

nucleophilic addition step (0.981). The observed HDVr $^{18}k_{NUC}$ of 1.024 is therefore likely to correspond to a large normal contribution from deprotonation, consistent with observations from substituent effects.[48] Given the large normal $^{18}k_{NUC}$ of 1.024 for HDVr, a significant inverse contribution due to O−P bond formation would require an offsetting EIE due to deprotonation of 3% or greater. However, EIEs of only 1−2% for deprotonation of a range of compounds have been documented.[54−56] For example, the EIE for deprotonation of nitrophenol was reported as 1.0153 and values in the range of 1.014−1.019 were measured for phosphoric acid and glucose phosphate.[56]

Using the remote label method, we measured an $^{18}k_{LG}$ for HDVr of 1.017, which can be compared to the results from non-enzymatic reactions of UpG and an 11 mer oligonucleotide catalyzed by hydroxide (Tables 1 and S1). The values of 1.034 for UpG and of 1.019 for the 11 mer in reactions catalyzed by hydroxide represent late transition states with advanced 5′O−P bond cleavage and no offsetting contribution from proton transfer. These values contrast with the $^{18}k_{LG}$ of 1.0064 measured for an activated nitrophenol leaving group reflecting an early TS.[49] Additionally, the $^{18}k_{LG}$ measured for non-enzymatic catalysis at a low pH (Table 1, pH 1) of 1.005 reflects an early TS for breakdown of a stable phosphorane intermediate.[21,22] Thus, the value of 1.017 for HDVr indicates significant bond cleavage in the transition state compared to results for non-enzymatic reactions catalyzed by hydroxide. Importantly, there is strong evidence that 5′O is acted on by C75 as the general acid.[41] Formation of a new 5′O−H bond due to general acid catalysis, as suggested by Brønsted effects,[40,57] would result in an inverse contribution to the observed $^{18}k_{LG}$, partially offsetting contributions from 5′O−P bond cleavage. Consequently, the observed $^{18}k_{LG}$ for HDVr underestimates the extent of bond cleavage in the transition state.

Both bonding and bending vibrational modes can influence the observed KIE on the nonbridging oxygens.[8] The substrate for measurement of $^{18}k_{NPO}$ is a mixture of diastereomers, so the observed KIE of 0.994 represents an average contribution of the fractionation for each NPO atom. This small inverse secondary KIE is consistent with an increased bond order to the NPO atoms, consistent with a transition state with partial metaphosphate-like character[8] that is more commonly associated with the reactions of phosphate monoesters.[19]

Together, normal primary KIEs on the leaving group and nucleophile combined with an inverse secondary isotope effect on the nonbridging oxygen(s) are consistent with a dissociative-like transition state where 5′O−P bond cleavage is more advanced than the formation of the 2′O−P bond. Moreover, the magnitudes of these KIEs in comparison to base-catalyzed cleavage impose significant offsetting contributions from proton transfers for the nucleophile and leaving group. This transition state is therefore distinct from non-enzymatic reactions and RNase A (Figure 3). RNase A provides rate enhancement by using acid/base catalysis to stabilize a transition state that is similar to non-enzymatic reactions under alkaline conditions as inferred by KIEs.[21,25] In contrast, HDVr provides rate enhancement using a combination of nucleobase and metal ion catalytic interactions. The KIE data demonstrate that the free energy surface for the HDVr reaction is distorted relative to ideal non-enzymatic reactions and RNase A toward a dissociative path and metaphosphate-like transition state marked by limited 2′O−P bond formation.

https://doi.org/10.1021/jacs.2c10079
J. Am. Chem. Soc. 2023, 145, 2830−2839

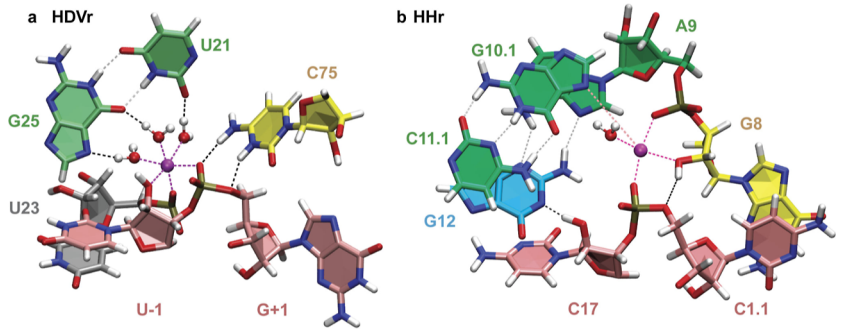

Figure 5. HDVr active site comparison. (a) HDVr active state and (b) HHr active state. HDVr and HHr active states use similar Mg^{2+} binding modes to enable different catalytic strategies (general base "γ" catalysis in HDVr and general acid "δ" catalysis in HHr).

Ab Initio QM/MM Calculations Confirm That Experimental KIEs Correspond to a Dissociative-like Transition State. Combined QM/molecular mechanical (MM) calculations were previously used to study the HDVr mechanism by Ganguly et al.[37] They concluded that HDVr employs a concerted mechanism that is synchronous with proton transfer and O2′/O5′-P bond breaking/forming occurring simultaneously and passing through a phosphorane-like transition state where the O2′−P and O5′-P distances are ∼1.8 and ∼2.2 Å, respectively.[37] In search for alternative mechanisms,[37] that study also reported another phosphorane-like transition state, 5 kcal/mol higher in the barrier, which had O2′−P and O5′−P bonds roughly equidistant (∼2.1 Å). KIE predictions were not reported, which is reasonable as there were no available experimental data at the time.

The goal of the calculations presented herein is to provide an interpretation of the experimentally measured KIEs in terms of the structure and bonding of the transition state. To achieve this, we first performed classical molecular dynamics simulations to identify the catalytically active state in solution, which serves as a departure point for the chemical steps of the reaction. Next, we used combined QM/MM free energy simulations to determine associative and dissociative pathways for the reaction. We found that the most plausible active state involved the Mg^{2+} ion making inner-sphere coordination to both the 2′O nucleophile and the pro-R_P NPO of the scissile phosphate, while C75 was protonated at the N3 position and forming hydrogen bonds with the pro-R_P NPO and the O5′ leaving group. Details are discussed in the Supporting Information and results shown in Figures S6 and S7. Finally, departing from the observed transition state ensembles of the QM/MM simulations, we performed ab initio QM/MM calculations (e.g., transition state optimizations) to pinpoint representative transition state structures for each pathway.

The two ab initio QM/MM optimized TS structures differ in both the bonding around the central phosphorus atom and the degree of proton transfer to the O5′ leaving group from the general acid, C75 (Figure 4). The associative TS is characterized by similar O2′−P and P−O5′ distances (1.86 and 1.97 Å, respectively) and bond orders (0.45 and 0.50, respectively) and partial proton transfer to the leaving group (H−O5′ bond order 0.35). The dissociative TS has a considerably longer O2′−P distance (2.51 Å) with a markedly lower bond order (0.21), and proton transfer to the leaving group is slightly more complete (H−O5′ bond order 0.41). Each TS yields substantially different KIEs calculated by vibrational frequency analysis (Table 1). The calculated primary KIEs for the dissociative mechanism agree very closely with the experimental values in terms of normal versus inverse direction and the magnitudes for both the primary nucleophile and the leaving group KIEs. Whereas the experimental secondary KIEs for the NPOs are mildly inverse and consistent with partial metaphosphate-like character (increased P−O bond order),[8] the calculated KIEs are closer to unity. Our computational findings support a model consistent with experiment where the O2′ directly coordinates the Mg^{2+}, enabling the enzyme and substrate to be in position to react. In this binding mode, Mg^{2+} acidifies the nucleophile, facilitating proton abstraction by specific base catalysis while stabilizing the activated nucleophile in the TS. This stabilization by Mg^{2+} is also likely the main factor causing the shift to a dissociative transition state, although further experimental and computational mechanistic work is needed before that can be definitively concluded.

Implications for Ribozyme Catalysis. HDVr is not the only ribozyme active site that contains a Mg^{2+} ion coordinated to both an NPO and a 2′OH, facilitating its deprotonation. The hammerhead ribozyme (HHr) appears to use this feature in leaving group stabilization (through activation of the 2′OH of G8 for general acid catalysis)[58,59] as opposed to the nucleophile activation seen in HDVr (Figure 5). Examples of common catalytic devices shared across ribozyme classes are beginning to emerge, as suggested from comparative structure analysis[60] and in-depth mechanistic studies.[61] One implication of these shared features is that ribozymes, with their limited repertoire of building blocks and available chemical functional groups, evolved distinct active site designs that stabilize altered transition states. Protein enzymes such as RNase A, on the other hand, have a richer set of building blocks and functional groups for catalytic optimization and may have diverged comparatively further.

CONCLUSIONS

Here we have shown that biomolecules capable of phosphoryl transfer transition states have not universally converged on catalytic pathways that proceed through a common distinct transition state; rather, multiple biologically feasible routes to RNA cleavage are possible, which can navigate through different transition states. The ability to obtain a chemically detailed description of 2′-*O*-transphosphorylation transition states through KIE analysis provides an opportunity to advance our understanding of biological catalysis. A broader analysis of isotope effects for ribozymes that bear precise atomic modifications and for other classes of ribozymes that have different active site configurations would unveil the link between transition state interactions and transition state

https://doi.org/10.1021/jacs.2c10079
J. Am. Chem. Soc. 2023, 145, 2830−2839

structure, providing unique insights into the diverse catalytic strategies found in biology.

■ ASSOCIATED CONTENT

Supporting Information

The Supporting Information is available free of charge at https://pubs.acs.org/doi/10.1021/jacs.2c10079.

Synthesis of ribozyme and isotopically enriched substrate RNAs, RNA reaction kinetics and binding commitments, measurement of kinetic isotope effects by remote label and mass spectrometry, computational methods including MM simulations of catalytic fitness, QM/MM free energy simulations of the RNA cleavage reaction, and ab initio QM/MM kinetic isotope effect calculations (PDF)

■ AUTHOR INFORMATION

Corresponding Authors

Michael E. Harris − *Department of Chemistry, University of Florida, Gainesville, Florida 32611, United States;* orcid.org/0000-0001-8977-4392; Email: harris@chem.ufl.edu

Darrin M. York − *Laboratory for Biomolecular Simulation Research, Institute for Quantitative Biomedicine, Department of Chemistry and Chemical Biology, Rutgers University, Piscataway, New Jersey 08854, United States;* orcid.org/0000-0002-9193-7055; Email: Darrin.York@rutgers.edu

Joseph A. Piccirilli − *Department of Chemistry and Department of Biochemistry and Molecular Biology, The University of Chicago, Chicago, Illinois 60637, United States;* orcid.org/0000-0002-0541-6270; Email: jpicciri@uchicago.edu

Authors

Benjamin Weissman − *Department of Chemistry and Department of Biochemistry and Molecular Biology, The University of Chicago, Chicago, Illinois 60637, United States;* orcid.org/0000-0003-0804-0464

Şölen Ekesan − *Laboratory for Biomolecular Simulation Research, Institute for Quantitative Biomedicine, Department of Chemistry and Chemical Biology, Rutgers University, Piscataway, New Jersey 08854, United States;* orcid.org/0000-0002-5598-5754

Hsuan-Chun Lin − *Department of Chemistry, University of Florida, Gainesville, Florida 32611, United States*

Shahbaz Gardezi − *Department of Chemistry, University of Florida, Gainesville, Florida 32611, United States*

Nan-Sheng Li − *Department of Chemistry and Department of Biochemistry and Molecular Biology, The University of Chicago, Chicago, Illinois 60637, United States;* orcid.org/0000-0002-1185-3688

Timothy J. Giese − *Laboratory for Biomolecular Simulation Research, Institute for Quantitative Biomedicine, Department of Chemistry and Chemical Biology, Rutgers University, Piscataway, New Jersey 08854, United States;* orcid.org/0000-0002-0653-9168

Erika McCarthy − *Laboratory for Biomolecular Simulation Research, Institute for Quantitative Biomedicine, Department of Chemistry and Chemical Biology, Rutgers University, Piscataway, New Jersey 08854, United States;* orcid.org/0000-0001-8089-0207

Complete contact information is available at: https://pubs.acs.org/10.1021/jacs.2c10079

Notes

The authors declare no competing financial interest.

■ ACKNOWLEDGMENTS

The authors are grateful for the financial support provided by the National Institutes of Health (GM127100 to M.E.H., GM062248 to D.M.Y., and GM131568 to J.A.P.). D.M.Y. is also grateful to Alan Grossman for providing early-stage seed support for our research through the Grossman Innovation Prize. Computational resources that have contributed to the research results reported within this work were provided by the Office of Advanced Research Computing (OARC) at Rutgers, The State University of New Jersey, the Extreme Science and Engineering Discovery Environment (XSEDE), which is supported by National Science Foundation grant ACI-1548562 (specifically, the resources EXPANSE at SDSC through allocation TG-CHE190067), and the Texas Advanced Computing Center (TACC, http://www.tacc.utexas.edu) at The University of Texas at Austin, specifically the Frontera Supercomputer.

■ REFERENCES

(1) Garcia-Viloca, M.; Gao, J.; Karplus, M.; Truhlar, D. G. How enzymes work: Analysis by modern rate theory and computer simulations. *Science* **2004**, *303*, 186−195.

(2) Schramm, V. L. Enzymatic Transition States and Drug Design. *Chem. Rev.* **2018**, *118*, 11194−11258.

(3) Arnold, F. H. Directed Evolution: Bringing New Chemistry to Life. *Angew. Chem., Int. Ed.* **2018**, *57*, 4143−4148.

(4) Bevilacqua, P. C.; Harris, M. E.; Piccirilli, J. A.; Gaines, C.; Ganguly, A.; Kostenbader, K.; Ekesan, Ş.; York, D. M. An Ontology for Facilitating Discussion of Catalytic Strategies of RNA-Cleaving Enzymes. *ACS Chem. Biol.* **2019**, *14*, 1068−1076.

(5) Emilsson, G. M.; Nakamura, S.; Roth, A.; Breaker, R. R. Ribozyme speed limits. *RNA* **2003**, *9*, 907−918.

(6) Kohen, A.; Limbach, H.-H. *Isotope Effects in Chemistry and Biology*; Taylor & Francis, 2006.

(7) Melander, L. C. S.; Saunders, W. H. *Reaction Rates of Isotopic Molecules*; R.E. Krieger Pub. Co., 1987.

(8) Hengge, A. C. Isotope effects in the study of phosphoryl and sulfuryl transfer reactions. *Acc. Chem. Res.* **2002**, *35*, 105−112.

(9) Kuimelis, R. G.; McLaughlin, L. W. Mechanisms of Ribozyme-Mediated RNA Cleavage. *Chem. Rev.* **1998**, *98*, 1027−1044.

(10) Bashkin, J. K. Introduction to RNA/DNA Cleavage. *Chem. Rev.* **1998**, *98*, 937−938.

(11) Sullenger, B. A.; Nair, S. From the RNA world to the clinic. *Science* **2016**, *352*, 1417−1420.

(12) Kim, C. M.; Smolke, C. D. Biomedical applications of RNA-based devices. *Curr. Opin. Biomed. Eng.* **2017**, *4*, 106−115.

(13) Yang, Z.; Hutter, D.; Sheng, P.; Sismour, A. M.; Benner, S. A. Artificially expanded genetic information system: a new base pair with an alternative hydrogen bonding pattern. *Nucleic Acids Res.* **2006**, *34*, 6095−6101.

(14) Liu, J.; Cao, Z.; Lu, Y. Functional Nucleic Acid Sensors. *Chem. Rev.* **2009**, *109*, 1948−1998.

(15) Weinberg, Z.; Kim, P. B.; Chen, T. H.; Li, S.; Harris, K. A.; Lünse, C. E.; Breaker, R. R. New classes of self-cleaving ribozymes revealed by comparative genomics analysis. *Nat. Chem. Biol.* **2015**, *11*, 606−610.

(16) Lilley, D. M. J. Classification of the nucleolytic ribozymes based upon catalytic mechanism. *F1000Research* **2019**, *8*, 1462.

(17) Rodnina, M. V. *Ribozymes and RNA Catalysis*; Lilley, D. M., Eckstein, F., Eds.; *RSC Biomolecular Series*; RSC Publishing, 2008; pp 270−294.

(18) Gesteland, R. F.; Cech, T. R.; Atkins, J. F. *The RNA World: The Nature of Modern RNA Suggests a Prebiotic RNA*; Cold Spring Harbor Laboratory Press, 1999.
(19) Lassila, J. K.; Zalatan, J. G.; Herschlag, D. Biological phosphoryl-transfer reactions: understanding mechanism and catalysis. *Annu. Rev. Biochem.* **2011**, *80*, 669−702.
(20) Chen, H.; Giese, T. J.; Huang, M.; Wong, K.-Y.; Harris, M. E.; York, D. M. Mechanistic Insights into RNA Transphosphorylation from Kinetic Isotope Effects and Linear Free Energy Relationships of Model Reactions. *Chem.—Eur. J.* **2014**, *20*, 14336−14343.
(21) Gu, H.; Zhang, S.; Wong, K.-Y.; Radak, B. K.; Dissanayake, T.; Kellerman, D. L.; Dai, Q.; Miyagi, M.; Anderson, V. E.; York, D. M.; et al. Experimental and computational analysis of the transition state for ribonuclease A-catalyzed RNA 2'-O-transphosphorylation. *Proc. Natl. Acad. Sci. U.S.A.* **2013**, *110*, 13002−13007.
(22) Harris, M. E.; Dai, Q.; Gu, H.; Kellerman, D. L.; Piccirilli, J. A.; Anderson, V. E. Kinetic Isotope Effects for RNA Cleavage by 2 '-O-Transphosphorylation: Nucleophilic Activation by Specific Base. *J. Am. Chem. Soc.* **2010**, *132*, 11613−11621.
(23) Chen, H.; Piccirilli, J. A.; Harris, M. E.; York, D. M. Effect of Zn^{2+} binding and enzyme active site on the transition state for RNA 2'-O-transphosphorylation interpreted through kinetic isotope effects. *Biochim. Biophys. Acta, Proteins Proteomics* **2015**, *1854*, 1795−1800.
(24) Zhang, S.; Gu, H.; Chen, H.; Strong, E.; Ollie, E. W.; Kellerman, D.; Liang, D.; Miyagi, M.; Anderson, V. E.; Piccirilli, J. A.; et al. Isotope effect analyses provide evidence for an altered transition state for RNA 2'-O-transphosphorylation catalyzed by Zn^{2+}. *Chem. Commun.* **2016**, *52*, 4462−4465.
(25) Harris, M. E.; Piccirilli, J. A.; York, D. M. Integration of kinetic isotope effect analyses to elucidate ribonuclease mechanism. *Biochim. Biophys. Acta* **2015**, *1854*, 1801−1808.
(26) Gaines, C. S.; Giese, T. J.; York, D. M. Cleaning Up Mechanistic Debris Generated by Twister Ribozymes Using Computational RNA Enzymology. *ACS Catal.* **2019**, *9*, 5803−5815.
(27) Lilley, D. M. J. How RNA acts as a nuclease: some mechanistic comparisons in the nucleolytic ribozymes. *Biochem. Soc. Trans.* **2017**, *45*, 683−691.
(28) Hiller, D. A.; Singh, V.; Zhong, M. H.; Strobel, S. A. A two-step chemical mechanism for ribosome-catalysed peptide bond formation. *Nature* **2011**, *476*, 236−239.
(29) Unrau, P. J.; Bartel, D. P. An oxocarbenium-ion intermediate of a ribozyme reaction indicated by kinetic isotope effects. *Proc. Natl. Acad. Sci. U.S.A.* **2003**, *100*, 15393−15397.
(30) Oivanen, M.; Kuusela, S.; Lönnberg, H. Kinetics and mechanisms for the cleavage and isomerization of the phosphodiester bonds of RNA by Bronsted acids and bases. *Chem. Rev.* **1998**, *98*, 961−990.
(31) Wong, K. Y.; Gu, H.; Zhang, S.; Piccirilli, J. A.; Harris, M. E.; York, D. M. Characterization of the reaction path and transition States for RNA transphosphorylation models from theory and experiment. *Angew. Chem., Int. Ed. Engl.* **2012**, *51*, 647−651.
(32) Ferré-D'Amaré, A. R.; Zhou, K.; Doudna, J. A. Crystal structure of a hepatitis delta virus ribozyme. *Nature* **1998**, *395*, 567−574.
(33) Kapral, G. J.; Jain, S.; Noeske, J.; Doudna, J. A.; Richardson, D. C.; Richardson, J. S. New tools provide a second look at HDV ribozyme structure, dynamics and cleavage. *Nucleic Acids Res.* **2014**, *42*, 12833−12846.
(34) Chen, J.-H.; Yajima, R.; Chadalavada, D. M.; Chase, E.; Bevilacqua, P. C.; Golden, B. L. A 1.9 A crystal structure of the HDV ribozyme precleavage suggests both Lewis acid and general acid mechanisms contribute to phosphodiester cleavage. *Biochemistry* **2010**, *49*, 6508−6518.
(35) Ganguly, A.; Bevilacqua, P. C.; Hammes-Schiffer, S. Quantum Mechanical/Molecular Mechanical Study of the HDV Ribozyme: Impact of the Catalytic Metal Ion on the Mechanism. *J. Phys. Chem. Lett.* **2011**, *2*, 2906−2911.
(36) Lee, T.-S.; Giambaşu, G. M.; Harris, M. E.; York, D. M. Characterization of the Structure and Dynamics of the HDV Ribozyme in Different Stages Along the Reaction Path. *J. Phys. Chem. Lett.* **2011**, *2*, 2538−2543.
(37) Ganguly, A.; Thaplyal, P.; Rosta, E.; Bevilacqua, P. C.; Hammes-Schiffer, S. Quantum Mechanical/Molecular Mechanical Free Energy Simulations of the Self-Cleavage Reaction in the Hepatitis Delta Virus Ribozyme. *J. Am. Chem. Soc.* **2014**, *136*, 1483−1496.
(38) Mlýnský, V.; Walter, N. G.; Šponer, J.; Otyepka, M.; Banáš, P. The role of an active site Mg(2+) in HDV ribozyme self-cleavage: insights from QM/MM calculations. *Phys. Chem. Chem. Phys.* **2015**, *17*, 670−679.
(39) Lee, T.-S.; Radak, B. K.; Harris, M. E.; York, D. M. A Two-Metal-Ion-Mediated Conformational Switching Pathway for HDV Ribozyme Activation. *ACS Catal.* **2016**, *6*, 1853−1869.
(40) Perrotta, A. T.; Wadkins, T. S.; Been, M. D. Chemical rescue, multiple ionizable groups, and general acid-base catalysis in the HDV genomic ribozyme. *RNA* **2006**, *12*, 1282−1291.
(41) Das, S. R.; Piccirilli, J. A. General acid catalysis by the hepatitis delta virus ribozyme. *Nat. Chem. Biol.* **2005**, *1*, 45−52.
(42) Chen, J.-H.; Gong, B.; Bevilacqua, P. C.; Carey, P. R.; Golden, B. L. A catalytic metal ion interacts with the cleavage site GU wobble in the HDV ribozyme. *Biochemistry* **2009**, *48*, 1498−1507.
(43) Gong, B.; Chen, J.-H.; Bevilacqua, P. C.; Golden, B. L.; Carey, P. R. Competition between $Co(NH_3)_6^{3+}$ and inner sphere Mg^{2+} ions in the HDV ribozyme. *Biochemistry* **2009**, *48*, 11961−11970.
(44) Gong, B.; Chen, J.-H.; Chase, E.; Chadalavada, D. M.; Yajima, R.; Golden, B. L.; Bevilacqua, P. C.; Carey, P. R. Direct measurement of a pKa near neutrality for the catalytic cytosine in the genomic HDV ribozyme using Raman crystallography. *J. Am. Chem. Soc.* **2007**, *129*, 13335−13342.
(45) Gong, B.; Chen, Y.; Christian, E. L.; Chen, J.-H.; Chase, E.; Chadalavada, D. M.; Yajima, R.; Golden, B. L.; Bevilacqua, P. C.; Carey, P. R. Detection of innersphere interactions between magnesium hydrate and the phosphate backbone of the HDV ribozyme using Raman crystallography. *J. Am. Chem. Soc.* **2008**, *130*, 9670−9672.
(46) Thaplyal, P.; Ganguly, A.; Golden, B. L.; Hammes-Schiffer, S.; Bevilacqua, P. C. Thio effects and an unconventional metal ion rescue in the genomic hepatitis delta virus ribozyme. *Biochemistry* **2013**, *52*, 6499−6514.
(47) Thaplyal, P.; Ganguly, A.; Hammes-Schiffer, S.; Bevilacqua, P. C. Inverse thio effects in the hepatitis delta virus ribozyme reveal that the reaction pathway is controlled by metal ion charge density. *Biochemistry* **2015**, *54*, 2160−2175.
(48) Lu, J.; Koo, S. C.; Weissman, B.; Harris, M. E.; Li, N.-S.; Piccirilli, J. A. Evidence that nucleophile deprotonation exceeds bond formation in the HDV ribozyme transition state. *Biochemistry* **2018**, *57*, 3465−3472.
(49) Humphry, T.; Iyer, S.; Iranzo, O.; Morrow, J. R.; Richard, J. P.; Paneth, P.; Hengge, A. C. Altered Transition State for the Reaction of an RNA Model Catalyzed by a Dinuclear Zinc(II) Catalyst. *J. Am. Chem. Soc.* **2008**, *130*, 17858−17866.
(50) Bigeleisen, J.; Mayer, M. G. Calculation of Equilibrium Constants for Isotopic Exchange Reactions. *J. Chem. Phys.* **1947**, *15*, 261−267.
(51) Ye, J.-D.; Li, N. S.; Dai, Q.; Piccirilli, J. A. The mechanism of RNA strand scission: an experimental measure of the Bronsted coefficient, beta nuc. *Angew. Chem., Int. Ed. Engl.* **2007**, *46*, 3714−3717.
(52) Humphry, T.; Forconi, M.; Williams, N. H.; Hengge, A. C. Altered mechanisms of reactions of phosphate esters bridging a dinuclear metal center. *J. Am. Chem. Soc.* **2004**, *126*, 11864−11869.
(53) Jones, J. P.; Weiss, P. M.; Cleland, W. W. Secondary ^{18}O isotope effects for hexokinase-catalyzed phosphoryl transfer from ATP. *Biochemistry* **1991**, *30*, 3634−3639.
(54) Rishavy, M. A.; Cleland, W. W. ^{13}C, ^{15}N, and ^{18}O equilibrium isotope effects and fractionation factors 1. *Can. J. Chem.* **1999**, *77*, 967−977.

https://doi.org/10.1021/jacs.2c10079
J. Am. Chem. Soc. 2023, 145, 2830−2839

(55) Hengge, A. C.; Hess, R. A. Concerted or stepwise mechanisms for acyl transfer reactions of p-nitrophenyl acetate? transition state structures from isotope effects. *J. Am. Chem. Soc.* **1994**, *116*, 11256−11263.
(56) Knight, W. B.; Weiss, P. M.; Cleland, W. W. Determination of equilibrium ^{18}O isotope effects on the deprotonation of phosphate and phosphate esters and the anomeric effect on deprotonation of glucose-6-phosphate. *J. Am. Chem. Soc.* **1986**, *108*, 2759−2761.
(57) Koo, S. C.; Lu, J.; Li, N. S.; Leung, E.; Das, S. R.; Harris, M. E.; Piccirilli, J. A. Transition State Features in the Hepatitis Delta Virus Ribozyme Reaction Revealed by Atomic Perturbations. *J. Am. Chem. Soc.* **2015**, *137*, 8973−8982.
(58) Thomas, J. M.; Perrin, D. M. Probing general acid catalysis in the hammerhead ribozyme. *J. Am. Chem. Soc.* **2009**, *131*, 1135−1143.
(59) Blount, K. F.; Uhlenbeck, O. C. The Structure-Function Dilemma of the Hammerhead Ribozyme. *Annu. Rev. Biophys. Biomol. Struct.* **2005**, *34*, 415−440.
(60) Seith, D. D.; Bingaman, J. L.; Veenis, A. J.; Button, A. C.; Bevilacqua, P. C. Elucidation of Catalytic Strategies of Small Nucleolytic Ribozymes from Comparative Analysis of Active Sites. *ACS Catal.* **2018**, *8*, 314−327.
(61) Ganguly, A.; Weissman, B. P.; Giese, T. J.; Li, N.-S.; Hoshika, S.; Rao, R.; Benner, S. A.; Piccirilli, J. A.; York, D. M. Confluence of theory and experiment reveals the catalytic mechanism of the Varkud satellite ribozyme. *Nat. Chem.* **2020**, *12*, 193−201.

Recommended by ACS

Mechanisms of Sugar Aminotransferase-like Enzymes to Synthesize Stereoisomers of Non-proteinogenic Amino Acids in Natural Product Biosynthesis

Sumire Kurosawa, Makoto Nishiyama, *et al.*

JANUARY 20, 2023
ACS CHEMICAL BIOLOGY

READ

Unusual Paradigm for DNA–DNA Recognition and Binding: "Socket-Plug" Complementarity

Fiona Yutong Huang, Dipankar Sen, *et al.*

JANUARY 27, 2023
JOURNAL OF THE AMERICAN CHEMICAL SOCIETY

READ

Direct Activation of the C(sp^3)–NH_2 Bond of Primary Aliphatic Alkylamines by a High-Valent $Co^{III,IV}_2(\mu\text{-}O)_2$ Diamond Core Complex

Yan Li, Dong Wang, *et al.*

JANUARY 23, 2023
JOURNAL OF THE AMERICAN CHEMICAL SOCIETY

READ

Dissecting the Ultrafast Stepwise Bidirectional Proton Relay in a Blue-Light Photoreceptor

Zijing Chen, Dongping Zhong, *et al.*

FEBRUARY 01, 2023
JOURNAL OF THE AMERICAN CHEMICAL SOCIETY

READ

Get More Suggestions >

https://doi.org/10.1021/jacs.2c10079
J. Am. Chem. Soc. 2023, 145, 2830−2839